COBEM 2021 26th International Congress of Mechanical Engineering
November 22-26, 2021, Virtual Congress, Brazil

COB-2021-0703
CHAOS CONTROL OF AN SMA TWO-BAR TRUSS WITH CONSTRAINED THERMAL ACTUATION

Dimitri Danulussi Alves Costa
Marcelo Amorim Savi
Universidade Federal do Rio de Janeiro, COPPE - Departament of Mechanical Engineering, 21.945.972, Rio de Janeiro - RJ, Brazil
dda.costa@mecanica.coppe.ufrj.br

Davide Bernardini
Giuseppe Rega
Università di Roma-La Sapienza, Department of Structural and Geotechnical Engineering, Via Antonio Gramsci 53, 00197, Rome, Italy

Abstract. *Smart structures are employed in various fields of engineering due to their adaptive behavior. This is achieved through the application of several strategies, including the design of multi-stable configurations and the use of smart materials. Shape memory alloys (SMAs) are one type of such materials due to the thermomechanical coupling of their properties. The use of such alloys introduces nonlinearities to the structure which can lead to a range of nonlinear behaviors including chaos. This complex behavior brings an opportunity to provide adaptability to the structure via the application of chaos control techniques. These methods are able to stabilize an unstable periodic orbit within the chaotic attractor with a small energy cost. The robustness of this approach is still not fully explored in the literature, especially in situations where SMA actuators are of concern with actuation constrained by the energy equation. This work explores the capabilities of SMA actuation in chaos control methods and investigates how different control strategies influence the controlled orbit stability, filling the lack of such studies in the literature. An SMA two-bar truss is investigated representing a multi-stable structure. The SMA thermomechanical behavior is modeled by a constitutive equation that takes into account hysteresis and the thermomechanical coupling due to phase transformations. Results show that, depending on the actuation, the dependency of the controlled orbit stability with energy transfer coefficients changes, and control properties are affected in different ways. Finally, a successful thermal control is achieved indicating that SMA thermal actuation can be applied successfully to such structures.*

Keywords: *Chaos control, shape memory alloy, smart structures, nonlinear dynamics.*

1. INTRODUCTION

Smart structures are present in a variety of engineering systems due to their adaptive behavior. Common examples of their application are in robotics (Villanueva *et al.*, 2011), medicine (Kuribayashi *et al.*, 2006), civil engineering structures like bridges (Janke, 2005), aerospace industry (Hartl and Lagoudas, 2007), energy harvesters (Lebedev *et al.*, 2011), among others.

The adaptability of these structures is accompanied by complex nonlinear dynamics. Hence, various behaviors may be observed such as multistability and chaos. In some cases, these complex responses can be seen as undesired and may jeopardize the operation of these structures as in machining (Wiercigroch and Krivtsov, 2001), drilling and bridges. On the other hand, these behaviors can be desired and designed to augment the structure such as in energy harvesters (Ai *et al.*, 2019; Arrieta *et al.*, 2010; Lebedev *et al.*, 2011), drilling (Wiercigroch, 2007), origami structures (Kuribayashi *et al.*, 2006), among others. In all cases, the knowledge of the system behavior and its control are crucial for its operation.

Chaos control methods are a powerful tool that proportionates the desired behavior of a system with a low energy cost by taking advantage of its dynamics (Fradkov and Evans, 2005). They are been employed in several engineering systems and can be seen as an alternative to provide adaptability of smart structures (Andrievskii and Fradkov, 2004; De Paula and Savi, 2012). Recently, the extended time-delayed feedback method (ETDF) is been studied in several cases (Barbosa *et al.*, 2015; Costa and Savi, 2018) and even outside of a chaotic behavior, opening alternatives for new potential applications. However, there are only a few studies that deal with the effects of actuation constraints and noise on these types of controllers.

The application of control always requires a source of actuation and an accessible parameter of the system. In this regard, smart materials are interesting alternatives to provide actuation exploiting their mutiphysical couplings. Shape memory alloy (SMAs) is an example of such materials that present thermomechanical couplings that can be exploited for actuation. Several works deal with the application of SMA as actuators (Ertel and Mascaro, 2010; Saunders *et al.*, 2016), however, they focus on eliminating the nonlinear behavior of the alloy (Song *et al.*, 2003) or only the thermal

behavior of the device (Webb and Lagoudas, 1998). Hence, there is still a need for the analysis of the complete thermomechanical behavior of SMA as actuators that include a proper description of hysteresis and thermomechanical couplings.

This work deals with the application of the ETDF to a smart structure by utilizing the thermomechanical properties of the SMA for actuation. An SMA two-bar truss is used as a typical system to test and analyze the stability of the controlled behavior and how it is affected by thermal constraints. A constitutive model proposed in Bernardini and Rega (2005) is employed to describe the thermomechanical behavior of SMAs, include the thermomechanical couplings. Results show that the system has a rich behavior including high period orbits, chaos, and multi-stability. The controller succeeds to stabilize the target periodic orbit embedded on a chaotic attractor of the system. Other works investigated the control of SMA two bar-truss where the actuation is not provided by the SMA itself (Bessa *et al.*, 2013). Recently, the ETDF has been applied to an SMA two bar-truss (Costa *et al.*, 2019) analyzing the influence of thermal constraints using a polynomial constitutive model to describe the SMA thermomechanical behavior, neglecting thermomechanical couplings and details about its hysteresis.

2. SMA TWO-BAR TRUSS MODEL

The literature presents several alternatives to describe SMA thermomechanical behavior. Bernardini and Rega (2005) proposed a model that allows the proper description of hysteresis and thermomechanical couplings of these alloys being of special interest to describe the dynamical behavior of SMAs. The model can be formulated by considering a Helmholtz free energy potential given by:

$$\mathcal{H} = \frac{k}{2}[\epsilon - sign(\epsilon)\delta\zeta]^2 + \left[c_p T\left[1 - \ln\left(\frac{T}{T_0}\right)\right] - \eta_0 T\right] + \mathcal{H}_0 - c_p T_0, \tag{1}$$

where k is an elastic constant, ϵ is the strain, $\zeta \in [0,1]$ is the volume fraction of the martensitic phase, T is the temperature, c_p is the heat capacity, $\mathcal{H}_0$, η_0 and T_0 are the reference energy, entropy and temperature respectively; δ is a parameter linked to the width of the hysteresis loop, and b is a coupling parameter between transformation and temperature rates. Furthermore, T_0 is usually taken as the mean of the starting temperatures of the forward (austenite to martensite) and reverse (martensite to austenite) transformations. The first term of the Eq. 1 represents the strain energy, the second term is the heat energy of the material and the other terms are constants related to the reference configuration.

By assuming that the alloy is homogeneous, a single point description is adopted, and the sample has the same temperature and volume fraction at any point of the structure. Moreover, both tensile and compression induce martensite are considered to have symmetrical properties. The heat exchange between the SMA and the ambient is purely convective, and only happens on the surface of the SMA body, leading to a heat loss $Q = h[T_e - T]$. A current I is considered to pass through the SMA element generating heat by Joule effect, and the SMA is considered to have the same resistance R for both phases, leading to a heat generation inside the bars of RI^2. By integrating over the SMA body, the energy and entropy balance equations can be written as:

$$\begin{aligned} \dot{E} &= F_{sma}\dot{\epsilon} + h[T_\infty - T] + RI^2, \\ T\dot{\eta} - \Gamma &= h[T_\infty - T] + RI^2, \end{aligned} \tag{2}$$

where E is the internal energy of the SMA, F_{sma} is the restoring force at the lumped mass, h is the convection coefficient already taking into account the SMA surface area, T_∞ is the ambient temperature, η is the entropy of the system and Γ is the dissipation function.

The dissipation function is assumed to be given by:

$$\Gamma = \Lambda\dot{\zeta} \quad \text{with} \quad \Lambda = \begin{cases} \Lambda_F, & \text{if } \dot{\zeta} > 0 \\ \Lambda_R, & \text{if } \dot{\zeta} < 0 \end{cases} \tag{3}$$

where Λ are the constitutive functions that are the thresholds that the thermomechanical forces need to overcome to activate phase transformations, and subscripts F and R indicate forward and reverse transformations, respectively. The Clausius-Duhen inequality is satisfied since the dissipation is always positive ($\Gamma > 0$), leading to $\Lambda_F > 0$ and $\Lambda_R < 0$. Hence, Λ can be defined as follows:

$$\Lambda_F = b\delta\left[\frac{T_{As}-T_{Ms}}{2} - \frac{\left[T_{Ms}-T_{Mf}\right]}{ln\left(\frac{2-a}{a}\right)}\Psi_F\right] > 0,$$
$$\Lambda_R = b\delta\left[-\frac{T_{As}-T_{Ms}}{2} - \frac{\left[T_{Af}-T_{Ms}\right]}{ln\left(\frac{2-a}{a}\right)}\Psi_R\right] < 0, \quad (4)$$

where subscription $M(A)$ indicates temperatures related to the forward (reverse) transformations, subscriptions $s(f)$ indicate temperatures related to the start (finish) of these transformations, b is a conversion parameter that relates to the total energy dissipated from a loading cycle, and a is a smoothing parameter that acts on the end and beginning of transformations. It is important to highlight that, as the volume fraction represents martensite, the forward transformation is considered to generate martensite while the reverse transformation is consider to generate austenite. Finally, Ψ_F (Ψ_R) is given by:

$$\Psi_F = \frac{1}{2}ln\left(\frac{[2-a][\zeta-\zeta_0]+a[1-\zeta]}{a[\zeta-\zeta_0]+[2-a][1-\zeta]}\frac{2-a}{a}\right) > 0,$$
$$\Psi_R = \frac{1}{2}ln\left(\frac{a[\zeta-\zeta_0]-[2-a]\zeta}{[2-a][\zeta-\zeta_0]-a\zeta}\frac{a}{2-a}\right) < 0, \quad (5)$$

where ζ_0 is the volume fraction where the transformation started, and is used to model incomplete transformations (sub loops).

By employing Eq. (2) and (3), and taking the time derivative of Eq. (1), one obtains:

$$\left(F_{SMA} - \frac{\partial\mathcal{H}}{\partial\epsilon}\right)\dot{\epsilon} - \left(\eta - \frac{\partial\mathcal{H}}{\partial T}\right)\dot{T} - \left(\frac{\partial\mathcal{H}}{\partial\zeta} + \Lambda\right)\dot{\zeta} = 0. \quad (6)$$

Using that Eq. (6) should hold for all values of $\dot{\epsilon}$, $\dot{\theta}$ and $\dot{\zeta}$, it is obtained:

$$F_{SMA} = k[\epsilon - sign(\epsilon)\delta\zeta],$$
$$\eta = c\,ln\left(\frac{\theta}{\theta_0}\right) + \eta_0,$$
$$\dot{\zeta} = \frac{\delta\mathcal{G}}{1+k\delta^2\mathcal{G}}[sign(\epsilon)k\dot{\epsilon}], \quad (7)$$

where $\mathcal{G}$ is defined as $(\partial\Lambda/\,\partial\zeta\,)^{-1}$ during transformations and 0 otherwise. And, by using Eq. (2) again:

$$\dot{T} = \Lambda\frac{\dot{\zeta}}{c_p} + \frac{h}{c_p}[T_\infty - T] + RI^2. \quad (8)$$

It is also important to mention that the model assumes parallelism of the transformation plateaus, resulting in:

$$T_{Af} = T_{Ms}\frac{T_{Mf}+T_{As}-T_{Ms}}{T_{As}}. \quad (9)$$

Finally, Eq. (4), (5), (7) and (8) define all the constitutive behavior of the SMA.

2.1 Dynamical model

An SMA two-bar truss is analyzed considering the constitutive model previously presented to describe the SMA thermomechanical behavior. Figure 1 shows the SMA two-bar truss that is composed of two bars joined on one end and fixed to the ground on the other by rotating supports separated by a distance of $2B$. The SMA bars have a reference length L_0 defined by the length of the bars when only martensite is present on their crystalline structure and there is no stress field applied to the structure. The bars also are raised by X of their horizontal position generating an angle ϕ. A sinusoidal excitation force F_{exc} is vertically applied to the joint of the bars and the mass of the system m is considered to be concentrated at the same point. A viscous dissipation is considered with a damping coefficient c, to describe other system dissipations, different from the hysteris. Under these assumptions, the balance of forces at the bar`s joint can be expressed as:

$$m\,\ddot{X} = -F_{SMA}\sin(\phi_t) + F_{exc} - c\dot{X}, \tag{10}$$

By using the constitutive model to describe the bar restoring force F_{SMA}, the set of governing equations is obtained:

$$\begin{aligned} m\ddot{X} &= -(k[\epsilon - sign(\epsilon)\delta\zeta])\sin(\phi) - c\dot{X} + F_{exc}, \\ \dot{\zeta} &= \frac{\delta\mathcal{G} sign(\epsilon) k\dot{\epsilon}}{1 + k\delta^2\mathcal{G}}, \\ \dot{T} &= \Lambda\frac{\dot{\zeta}}{c_p} + \frac{h}{c_p}[T_\infty - T] + RI^2 \end{aligned} \tag{11}$$

By using the geometric identity $\epsilon = \sqrt{X^2 + B_t^2} - L_0$ and $\sin(\phi) = X/\sqrt{X^2 + B_t^2}$, defining $V \equiv \dot{X}$ and assuming a sinusoidal excitation, the equations of motion are given by :

$$\begin{aligned} \dot{X} &= V \\ \dot{V} &= -\frac{k\left[\sqrt{X^2 + B_t^2} - L_0 - \text{sign}\left(\sqrt{X^2 + B_t^2} - L_0\right)\delta\zeta\right]\text{X}}{m\sqrt{X^2 + B_t^2}} - \frac{c}{m}V + \frac{A\cos(\omega t)}{m}, \\ \dot{\zeta} &= \frac{\delta\mathcal{G}\ \text{sign}\left(\sqrt{X^2 + B_t^2} - L_0\right)kVX}{[1 + k\delta^2\mathcal{G}]\sqrt{X^2 + B_t^2}}, \\ \dot{T} &= \Lambda\frac{\dot{\zeta}}{c_p} + \frac{h}{c_p}[T_\infty - T] + RI^2. \end{aligned} \tag{12}$$

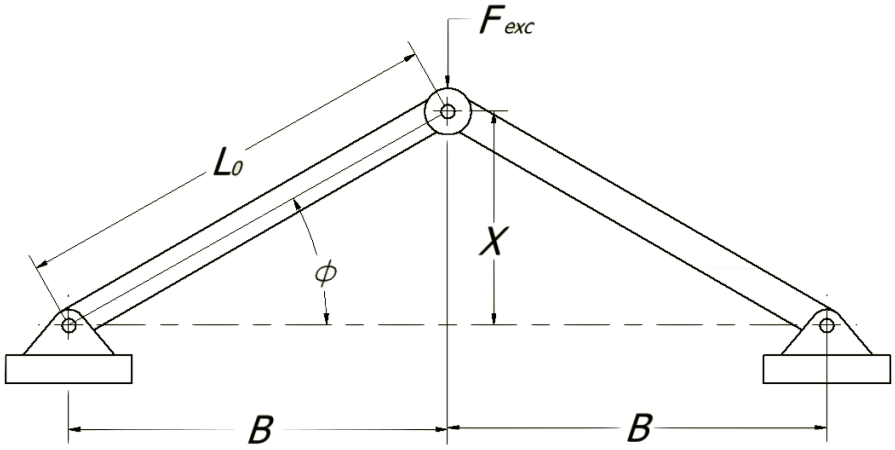

Figure 1. Schematic diagram of the two-bar truss on its reference position.

By considering non-dimensional parameters, the equations of motion can be rewritten:

$$\begin{aligned} x` &= v, \\ v' &= -\frac{\left[\sqrt{x^2 + b_t^2} - l_0 - sign\left(\sqrt{x^2 + b_t^2} - l_0\right)\delta^*\zeta\right]x_t}{\sqrt{x_t^2 + b_t^2}} - c^*v + A^*cos(\omega^* t^*), \\ \zeta' &= \frac{\delta^*\mathcal{G}^*}{1 + \delta^{*2}\mathcal{G}^*}\left[\frac{sign\left(\sqrt{x^2 + b_t^2} - l_0\right)vx}{\sqrt{x^2 + b_t^2}}\right], \\ \theta' &= \frac{L\Lambda^*}{J\delta^*}\zeta' + h^*[\theta_\infty - \theta] + R^*I^2, \end{aligned} \tag{13}$$

with,

$$\Lambda^* = \begin{cases} \Lambda_F = [J^* - 1]\delta^* \left[\dfrac{q_2 - 1}{2} - \dfrac{[1 - q_1]}{\ln\left(\dfrac{2-a}{a}\right)} \Psi_{\mathrm{F}} \right], & if\ \dot{\zeta} > 0 \\ \Lambda_R = [1 - J^*]\delta^* \left[-\dfrac{q_2 - 1}{2} - \dfrac{q_2[1 - q_3]}{\ln\left(\dfrac{2-a}{a}\right)} \Psi_{\mathrm{R}} \right], & if\ \dot{\zeta} < 0 \end{cases} \tag{14}$$

and,

$$\mathcal{G}^* = \begin{cases} \mathcal{G}_F^* = \dfrac{\ln\left(\dfrac{2-a}{a}\right)}{[J^* - 1]\delta^*[1 - q_1]} \left[\dfrac{\partial \Psi_F}{\partial \zeta}\right]^{-1}, & if\ \dot{\zeta} > 0 \\ \mathcal{G}_R^* = \dfrac{\ln\left(\dfrac{2-a}{a}\right)}{[1 - J^*]\delta^* q_2[1 - q_3]} \left[\dfrac{\partial \Psi_R}{\partial \zeta}\right]^{-1}, & if\ \dot{\zeta} < 0 \end{cases} \tag{15}$$

where $\omega_0 = \sqrt{\frac{k}{m}}$, $x = \frac{X}{X_{Ms}}$, $\theta = \frac{T}{T_0}, \theta_\infty = \frac{T_\infty}{T_0}$, $\delta^* = \frac{\delta}{X_{Ms}}$, $b_t = \frac{B}{X_{Ms}}$, $l_0 = \frac{L_0}{X_{Ms}}$, $f_{MS} = kX_{MS}$, $A^* = \frac{A}{f_{Ms}}$, $c^* = \frac{c}{\sqrt{k_e m_t}}$, $\omega^* = \frac{\omega}{\omega_0}$, $t^* = \omega_0 t$, $h^* = \frac{h}{c_p \omega_0}$, $\mathcal{G}^* = \frac{\mathcal{G}}{f_{Ms} X_{Ms}}$, $\Lambda^* = \frac{\Lambda}{X_{Ms} f_{Ms}}$, $q_1 = \frac{T_{Mf}}{T_{Ms}}$, $q_2 = \frac{T_{As}}{T_{Ms}}$, $q_3 = \frac{T_{Af}}{T_{Ms}}$, $v = \frac{V}{x_{Ms}\omega_0}$, $J^* = \frac{T_0 b}{f_{Ms}}$, $L^* = \frac{b\delta}{c_p}$ and X_{MS} is the height of the bars at the reference configuration.

Hence, Eq. (13), (14) and (15) are used to describe the system dynamics and in the numerical simulations.

2.2 Control and actuation model

The controller uses the time delayed-feedback method (Socolar *et al.*, 1994) and the control signal is defined by the feedback of delayed observation of the system which can be written as:

$$\boldsymbol{g} = \boldsymbol{K}\left([1 - R] \sum_{j=1}^{\infty} R^{j-1} \boldsymbol{y}(t - j\tau) - \boldsymbol{y}(t) \right), \tag{16}$$

where $\boldsymbol{K}$ is the gain of the controller and a positive definite matrix, R is a control parameter that is related to the influence of previous states, $\boldsymbol{g}$ is the control signal and $\boldsymbol{y}$ is the observation of the system. For the case in study the observation of the system is only related to its velocity and the temperature time evolution is the only directly accessible equation for the control. Hence, the control signal g, the gain K and the observable y are considered as scalars.

The current is the accessible parameter for the control to actuate the system. Hence, an ideal relation between the current and control signal can be defined as:

$$R^* I^2 = g = K\left([1 - R] \sum_{j=1}^{\infty} R^{j-1} \boldsymbol{y}(t - j\tau) - \boldsymbol{y}(t) \right), \tag{17}$$

It is important to highlight that as the actuation is provided by a current trough Joule effect, two controllers are taken into consideration: an ideal controller that can access even negative values of current; and a constrained controller that can access only positive values of the current $R^* I^2 \geq 0$. Hence the constrained controller can only be used in heating processes and it is actuation is defined by:

$$R^* I^2 = \begin{cases} g, & if \quad g \geq 0 \\ 0, & if \quad g < 0 \end{cases} \tag{18}$$

The evaluation of the controllers and the determination of parameters K and R are made by the analysis of the Floquet exponents of the controlled target orbit by the methods described in Costa *et al*. (2019) and Pyragas (2006). In summary, the maximum Floquet exponent real part of an orbit μ_{max} is evaluated. If μ_{max} is positive, the orbit is unstable, while, if μ_{max} is negative or zero, the orbit is stable. Based on that, as μ_{max} increases the targeted controlled orbit loses stability.

3. NUMERICAL SIMULATIONS

Numerical simulations are carried out by utilizing a fourth order Runge-Kutta method with a time step that guarantees a numerical precision of at least 10^{-10} estimated by a fifth order Runge-Kutta method. The parameters taken for the simulations are based on the literature and are found in Bernardini and Rega (2005). Table 1 summarizes all the parameter values.

Table 1. Parameter values for the SMA two-bar truss model.

Parameter	Value	Parameter	Value	Parameter	Value	Parameter	Value
l_0	18.00	J^*	3.1742	θ_∞	1.00	q_1	0.98
b	12.00	L^*	0.10	h*	0.02	q_2	1.20
μ^*	0.03	a	0.10	R^*	1.00	q_3	$1.01\overline{6}$
A^*	0.70	δ^*	3.8162				

3.1 System dynamics

Initially, the uncontrolled system dynamics is explored to identify a chaotic behavior. A bifurcation diagram with ω^* as the branching parameter is constructed and presented in Figure 2. The bifurcation diagram in displays a period-1 (Figure 2b), period-3 (Figure 2c), chaotic (Figure 2d) and period-2 (Figure 2e) solutions. Also, a periodic window inside the chaotic region can be seen around $\omega^* = 0.475$. Since temperature is a state variable, one can verify the orbits as a state-space subspace, temperature-position, for instance. Note that the chaotic structure observed through velocity-position plane has a better defined lamellar structure than in the temperature-position plane, however the behavior is confirmed to be chaotic.

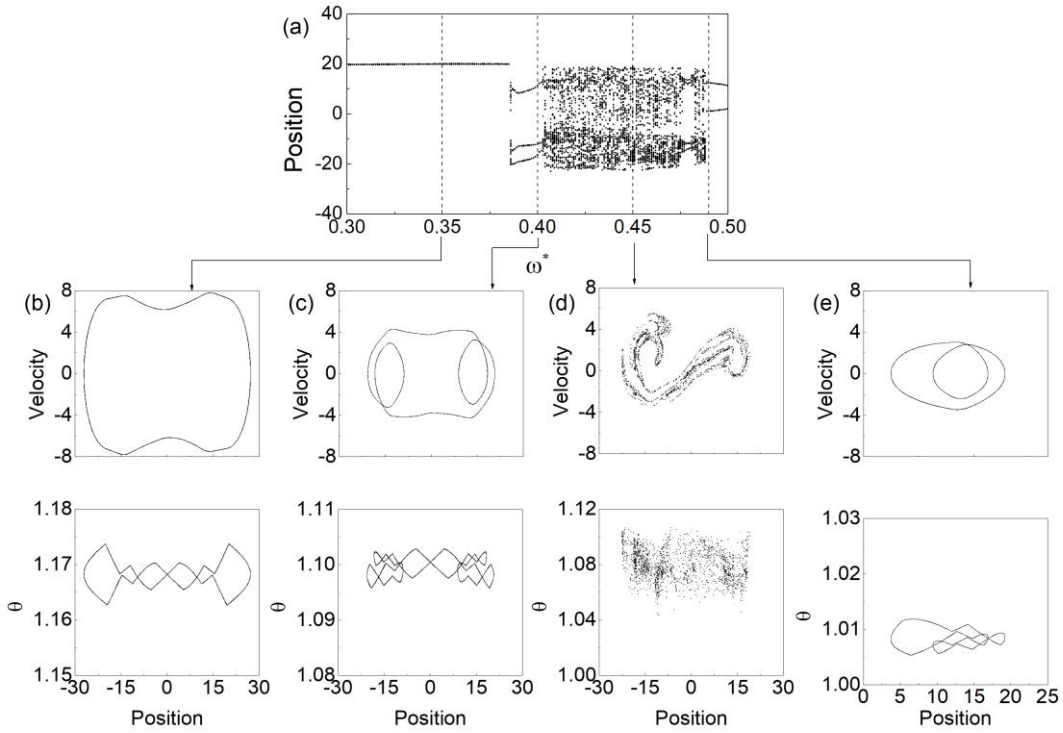

Figure 2. Dynamics with $h^* = 0.02$ for identification of chaotic regions to be controlled. (a) Bifurcation diagram. (b) State-space projections of the period-1 orbit at $\omega^* = 0.335$. (c) State-space projections of the period-3 orbit at $\omega^* = 0.4$. (d) Chaotic attractor at $\omega^* = 0.45$. (e) State-space projections of the period-2 orbit at $\omega^* = 0.49$. Vertical dashed black lines indicate frequencies where state-spaces are taken.

The chaotic region presented in Figure 2d is chosen to be analyzed to extract the unstable periodic orbits that will be controlled. Figure 3 presents the identified orbits where it is important to notice that each orbit has a reflected counterpart due to the system symmetry. The period-1 unstable periodic orbits are then chosen to be controlled.

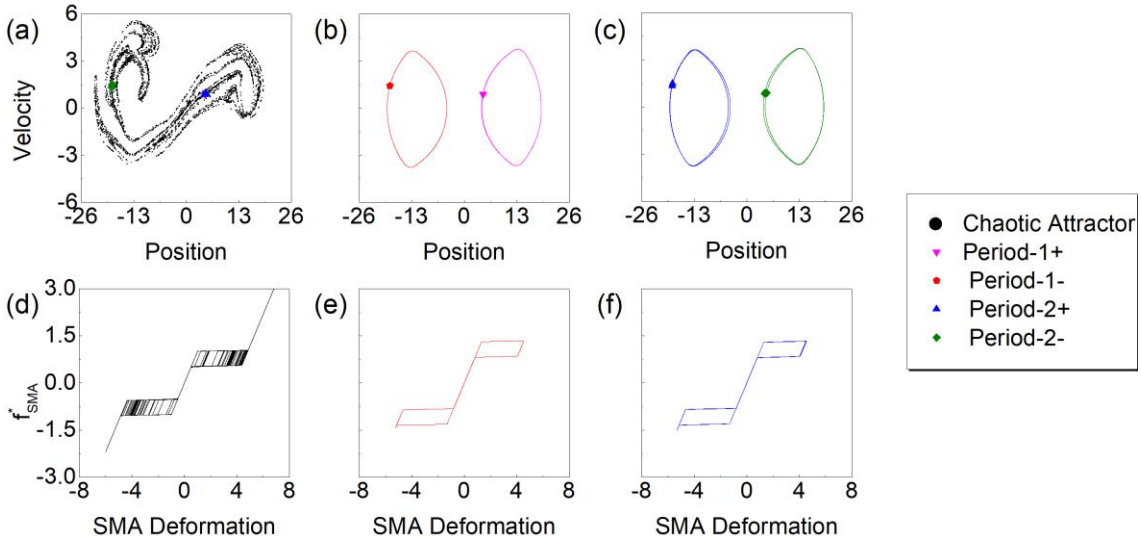

Figure 3. Chaotic attractor and unstable periodic orbits at $\omega^* = 0.45$ for the full model with $h^* = 0.02$. (a) Chaotic attractor and highlighted Poincaré sections of the identified UPOs. State-space of period-1 (b) and period-2 (c) identified UPOs. (d),(e),(f) Deformation versus force for the chaotic attractor, period-1 and period-2 UPOs respectively.

3.2 Control

The controller is employed to stabilize period-1 unstable periodic orbit by setting the parameters $R = 0.01$ and $K = 0.018$. The system is initialized in the neighborhood of the target orbit to avoid long transient solutions. Also, both ideal and constrained controllers are initialized at the same point to avoid the influence of initial conditions. Finally, both controllers only consider the first 10 terms of Eq. 17 as the infinity sum is considered to be rapidly convergent. Results for the ideal and constrained controller can be seen in Figure 4 to the left and right, respectively.

The ideal control quickly stabilizes the orbit (Figure 4a and Figure 4c) under 15 cycles of excitation, however the control signal does not go to zero after stabilization, this is due to the SMA behavior, as the coupling between temperature and velocity is only present when phase transformation occurs inside the SMA. In other words, when the system is in the linear behavior between deformation and force, which can be seen around zero deformation in Figure 4j, the mechanical part of the system is uncontrollable, and when phase transformation exist (hysteresis cycles on Figure 4j) the mechanical part of the system can be controlled. Hence, after stabilization, the mechanical part of the system still moves away from the target orbit when the is no phase transformations, and afterward, these deviations are corrected by the control signal in the presence of phase transformation. The ideal control Poincaré time series (Figure 4e) presents a transient damped sinusoidal behavior leading to a μ_{max} of $-0.04\ \mathrm{s}^{-1}$.

The constrained controller takes a larger time to stabilize the orbit of about 22 excitation cycles. The control signal does not vanish due to the same reasons of the ideal control. It presents a slightly higher variation when compared to the ideal control signal. The Poincaré time series of the controlled system presents a different behavior than the ideal case, as it displays a sinusoidal damping solution added with an exponential decay solution. This combined behavior is present when two Floquet exponents have similar positive real parts (Costa *et al.*, 2019). By analyzing time series, a μ_{max} of $-0.02\ \mathrm{s}^{-1}$ is obtained confirming that the constrained controller provides a higher μ_{max} than the ideal one, and hence, cannot provide the same level of stabilization as the ideal controller. Further investigating the constrained controller, one can verify that the exponential decay is related to the thermal part of the system while the damped sinusoidal decay is related to the mechanical part of the system. This indicates that the actuation constraints actually transferred the part of the system that is responsible for μ_{max}. In other words, the ideal controller has a μ_{max} related to the mechanical part of the system while the constrained controller has a μ_{max} related to the thermal part of the system as it is unable to provide cooling effects.

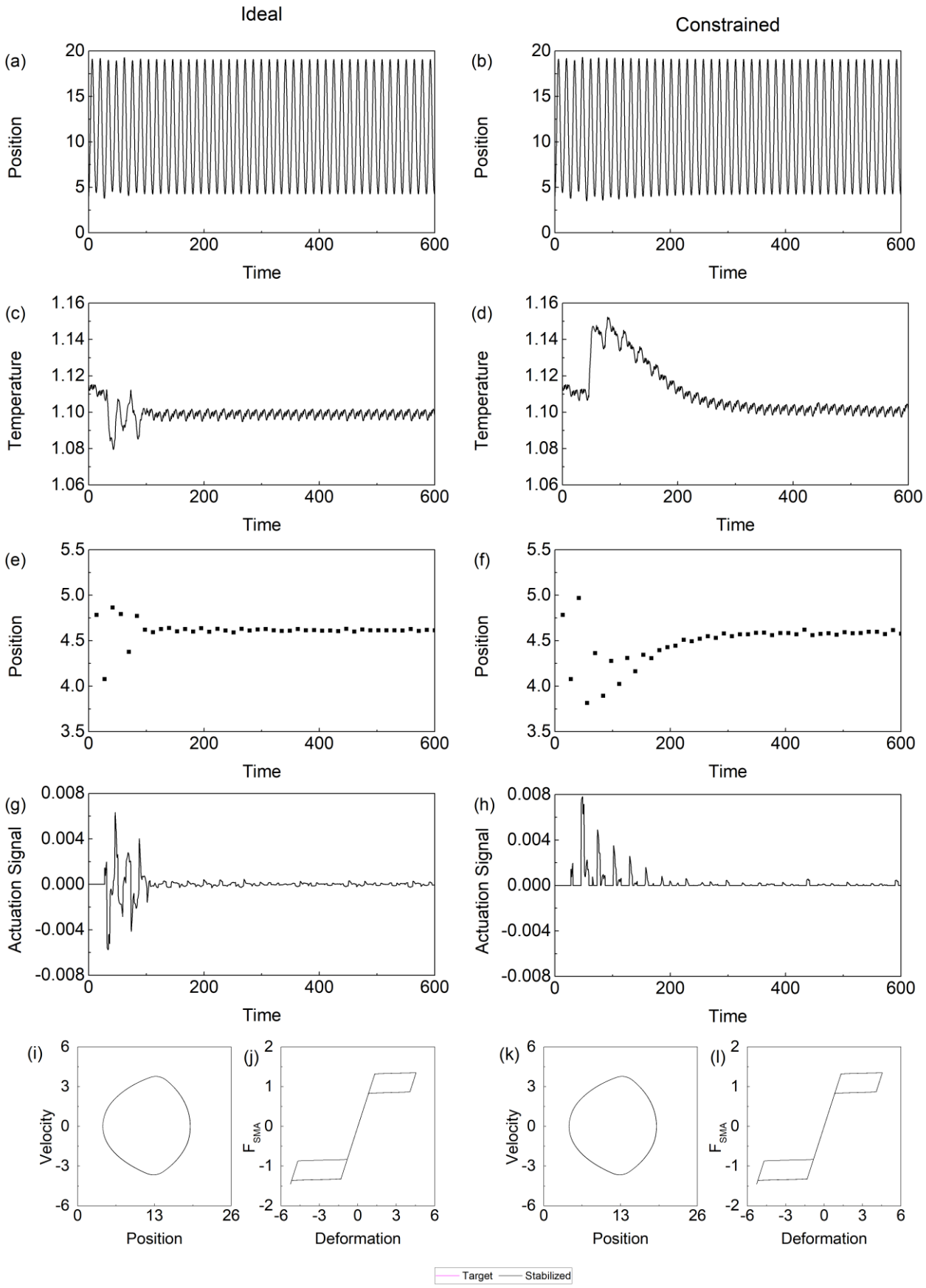

Figure 4. Ideal and constrained control of the period-1 UPO. (a,b) Position time history. (c,d) Temperature time history. (e,f) Poincaré time history. (g,h) Actuation signal time history. (i,k) Stabilized and targeted UPO. (j,l) SMA force versus deformation of the stabilized orbits.

4. CONCLUSIONS

This work investigated the constrained actuation using SMA elements on a smart structure. An SMA two-bar truss is used to test the control method and actuation and analyze how thermal constraints can influence the controlled orbit stability. The SMA constitutive behavior is constructed to include hysteresis and thermomechanical coupling effects due to phase transformation. The control method used is the extended time-delayed feedback method and it is considered that a current passing through the SMA is the accessible parameter. Results show that the control method can successfully stabilize the targeted orbit even when constrained to just positive values of actuation. The comparison between ideal and constrained controllers showed that if cooling effects are not controlled the maximum real-valued Floquet exponent μ_{max} of the orbit may depend on temperature instead of the mechanical part of the system. Finally, results showed that chaos control can be effectively applied to a smart structure with SMA elements, but a constrained actuation can lead to a lower stability of the orbit and should be studied in the design of the controller.

5. ACKNOWLEDGEMENTS

The authors would like to acknowledge the financial support of CNPq, CAPES and FAPERJ.

6. REFERENCES

Ai, R., Monteiro, L., Monteiro, P., Pacheco, P. and Savi, M. A., 2019. "Piezoelectric Vibration-Based Energy Harvesting Enhancement Exploiting Nonsmoothness." *Actuators*, v. 8, n. 1, p. 25.

Andrievskii, B. R. and Fradkov, A. L. , 2004. "Chaos Control Methods and Applications II. Applications." *Automation and Remote Control*, v. 65, n. 4, p. 505–533.

Arrieta, A. F., Hagedorn, P., Erturk, A. and Inman, D. J., 2015. "A piezoelectric bistable plate for nonlinear broadband energy harvesting." *Applied Physics Letters*, v. 97, n. 10.

Barbosa, W. O. V., De Paula, A. S., Savi, M. A. and Inman, D. J., 2015. "Chaos control applied to piezoelectric vibration-based energy harvesting systems." *The European Physical Journal Special Topics*, v. 224, n. 14–15, p. 2787–2801.

Bernardini, D. and Rega, G, 2005. "Thermomechanical modelling, nonlinear dynamics and chaos in shape memory oscillators." *Mathematical and Computer Modelling of Dynamical Systems*, v. 11, n. 3, p. 291–314.

Bessa, W. M., De Paula, A. S. and Savi, M. A. Adaptive fuzzy sliding mode control of smart structures. *The European Physical Journal Special Topics*, v. 222, n. 7, p. 1541–1551, 2013.

Costa, D. D. A. , Savi, M. A., de Paula, A. S. and Bernardini, D., 2019. "Chaos control of a shape memory alloy structure using thermal constrained actuation." *International Journal of Non-Linear Mechanics*.

Costa, D. D. A. and Savi, M. A., 2018. "Chaos control of an SMA–pendulum system using thermal actuation with extended time-delayed feedback approach." *Nonlinear Dynamics*, v. 93, n. 2, p. 571–583.

De Paula, A. S. and Savi, M. A., 2012. "Chaos Control Applied to Mechanical Systems." *Chaotic Modeling and Simulation (CMSIM)*, v. 1, p. 17–24.

Ertel, J. D. and Mascaro, S. A., 2010. "Dynamic Thermomechanical Modeling of a Wet Shape Memory Alloy Actuator." *Journal of Dynamic Systems, Measurement, and Control*, v. 132, n. 5, p. 051006.

Fradkov, A. L. and Evans, R. J., 2005. "Control of chaos: Methods and applications in engineering." *Annual Reviews in Control*, v. 29, n. 1, p. 33–56.

Hartl, D. J. and Lagoudas, D. C., 2007. "Aerospace applications of shape memory alloys." *Proceedings of the Institution of Mechanical Engineers, Part G: Journal of Aerospace Engineering*, v. 221, n. 4, p. 535–552.

Janke, L., 2005. "Applications of shape memory alloys in civil engineering structures - Overview, limits and new ideas." *Materials and Structures*, v. 38, n. 279, p. 578–592.

Kuribayashi, K., Tsuchya, K., You, Z., Tomus, D., Umemoto, M., Ito, T. and Saaki, M., 2006. "Self-deployable origami stent grafts as a biomedical application of Ni-rich TiNi shape memory alloy foil." *Materials Science and Engineering: A*, v. 419, n. 1–2, p. 131–137.

Lebedev, G. A., Gusarov, B. V., Viala, B., Delamare, J., Cugat, O., Lafont, T. and Zakharov, D. I., 2011. "Thermal energy harvesting using shape memory/piezoelectric composites." *Solid-State Sensors, Actuators and Microsystems Conference* (TRANSDUCERS), 2011 16th International. Anais...IEEE.

Pyragas, K., 2006. "Delayed feedback control of chaos." *Philosophical Transactions of the Royal Society A: Mathematical, Physical and Engineering Sciences*, v. 364, n. 1846, p. 2309–2334.

Saunders, R. N., Boyd,J. G., Hartl, D. J., Brown, J. K., Calkins, F. T. and Lagoudas, D. C., 2016. "A validated model for induction heating of shape memory alloy actuators." *Smart Materials and Structures*, v. 25, n. 4, p. 045022.

Socolar, J. E. S., Sukow, D. W. and Gauthier, D. J., 1994. "Stabilizing unstable periodic orbits in fast dynamical systems." *Physical Review E*, v. 50, n. 4, p. 3245–3248.

Song, G., Chaudhry, V. and Batur, C., 2003. "Precision tracking control of shape memory alloy actuators using neural networks and a sliding-mode based robust controller." *Smart materials and structures*, v. 12, n. 2, p. 223.

Villanueva, A., Smith, C. and Priya, S., 2011. "A biomimetic robotic jellyfish (Robojelly) actuated by shape memory alloy composite actuators." *Bioinspiration & Biomimetics*, v. 6, n. 3, p. 036004.

Webb, G. V. and Lagoudas, D. C., 1998. "Hysteresis Model of SMA Actuators for Control Applications." *Journal of Intelligent Material Systems and Structures*, v. 9, p. 432–448.

Wiercigroch, M., 2007. "Resonance enhanced drilling: method and apparatus." Patent No. WO2007141550.

Wiercigroch, M. and Krivtsov, A. M., 2001. "Frictional chatter in orthogonal metal cutting." *Philosophical Transactions of the Royal Society of London. Series A: Mathematical, Physical and Engineering Sciences*, v. 359, n. 1781, p. 713–738.

7. RESPONSIBILITY NOTICE

The authors are the only responsible for the printed material included in this paper.